Special Article

The 64th CerSJ Awards for Advancements in Ceramic Science and Technology: Review

Structural and dielectric properties of epitaxial (Ba,Sr)TiO₃ films on *c*-Al₂O₃ with ultra-thin TiN sacrificial template

Tomoaki YAMADA[†]

Department of Materials, Physics and Energy Engineering, Nagoya University, Furo-cho, Chikusa-ku, Nagoya 464–8603

Using ultra-thin TiN sacrificial template, the epitaxial (Ba,Sr)TiO₃ [BST] films on *c*-Al₂O₃ were grown by pulsed laser deposition. TiN epitaxially grew on *c*-Al₂O₃ with (111) orientation, which promoted the (111) epitaxial growth of upper BST films. The obtained epitaxial BST films showed significantly larger dielectric constant compared with polycrystalline films directly deposited on *c*-Al₂O₃ over the wide temperature range. By inserting the TiN template, the temperature corresponding to maximum dielectric constant of BST films was shifted up by 50 K, which is mainly due to the in-plane tensile strain induced by the difference in thermal expansion coefficients of BST and *c*-Al₂O₃.
©2011 The Ceramic Society of Japan. All rights reserved.

1. Introduction

Ferroelectric materials being in the paraelectric phase show the large change in dielectric constant by applying an electric field, which is attractive for the use in reconfigurable circuits.[1),2)] It is also known that these materials show fast-response, low-noise and competitive-loss level[3)] at high frequency ranges; therefore, the wide variety of applications used at radio and microwave frequencies can be expected.

Among these materials, (Ba$_x$Sr$_{1-x}$)TiO₃ [BST] is one of the most promising candidates.[1)–3)] BST films on dielectric substrates can be used for planar tunable capacitors and phase shifters. However, since the tunabilities of such planar structures are significantly lower than the tunability of BST itself due to the existence of substrate and air capacitances,[4)] a larger dielectric constant would be necessary for BST. Moreover, a ferroelectric material with a large dielectric constant will have a large tunability due to the strong physical correlation between tunability and dielectric constant.[2)]

Achieving a large dielectric constant in the film form is challenging as the dielectric constant of ferroelectric films is sensitively affected by structural factors such as porosity, grain size, crystallinity and strain.[5)–12)] Epitaxial growth would meet the most of required factors, which can be usually achieved by the selection of suitable substrates.[13),14)] However, the selection of substrates is critically limited from the viewpoint of practical applications. Sapphire (Al₂O₃) is one of few possible single crystal wafers. Although it has a large lattice mismatch with BST, some of the reported BST films show the epitaxial growth on *c*-Al₂O₃ [i.e., (0001) Al₂O₃] using metal–organic chemical vapor deposition[15)] and sputtering.[16)] On the other hand, polycrystalline films have been also often reported,[17),18)] which implies the importance of the growth control for such an unmatched interface.

We have reported that the ultra-thin TiN template on *c*-Al₂O₃ enabled the epitaxial growth of BST films with (111)-orientation[19)] (see **Fig. 1**). The required minimum thickness of TiN can

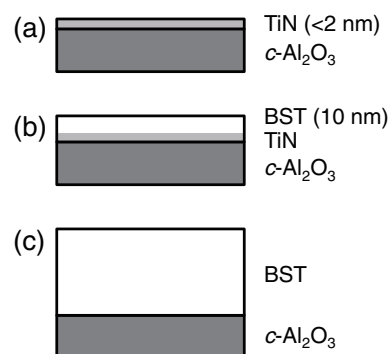† Corresponding author: T. Yamada; E-mail: t-yamada@nucl.nagoya-u.ac.jp

Fig. 1. Process flow of epitaxial BST films on *c*-Al₂O₃ using ultra-thin TiN sacrificial template: deposition of epitaxial ultra-thin TiN layer (<2 nm) at room temperature (a), deposition of epitaxial BST film at 720°C in vacuum for the first 10 nm (b), and contentious deposition of BST at 7 × 10⁻² Pa oxygen (c).

be less than 1 nm, and this ultra-thin template is sacrificially absorbed by BST films. In this paper, we report the comprehensive study on the structural and dielectric properties of BST films epitaxially grown on *c*-Al₂O₃ using ultra-thin TiN sacrificial template. The obtained epitaxial BST films show significantly larger dielectric constant than the polycrystalline films over the wide temperature range. In order to clarify the role of TiN template, the TiN thickness dependences of epitaxial growth, residual strain and dielectric constant of BST films are discussed.

2. Experimental

BST films and TiN templates were deposited on *c*-Al₂O₃ substrates by pulsed laser deposition with KrF excimer laser ($\lambda = 248$ nm). BST (x = 0.3) and TiN ceramics were used as targets. Following TiN deposition in vacuum at room temperature, BST was deposited at 720°C keeping vacuum for the first 10 nm in order to maintain the epitaxial TiN surface; then, oxygen was introduced to be 7 × 10⁻² Pa for the further deposition (Fig. 1). After the BST deposition, the samples were kept in air at 350°C for 1 h. For the comparison, the BST films

Fig. 2. XRD θ–2θ patterns of BST films directly deposited on *c*-Al₂O₃ at oxygen pressures of 13 Pa (a) and 7×10^{-2} Pa (b).
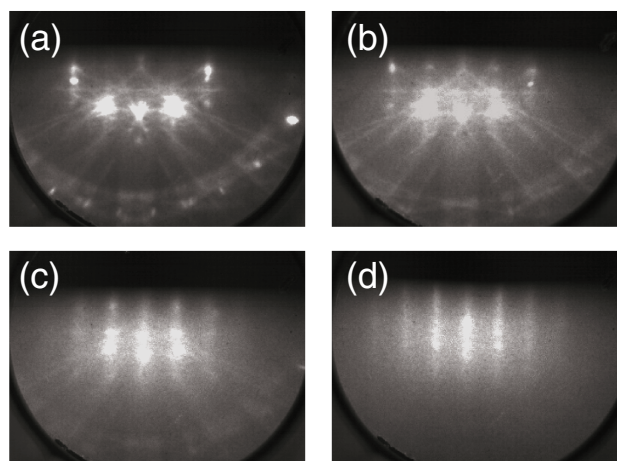

Fig. 3. RHEED images from *c*-Al₂O₃ surfaces covered with/without TiN layer: bare *c*-Al₂O₃ (a), 0.6 nm-thick TiN-covered *c*-Al₂O₃ (b), 0.9 nm-thick TiN-covered *c*-Al₂O₃ (c), and 1.8 nm-thick TiN-covered *c*-Al₂O₃ (d).

were directly deposited on *c*-Al₂O₃ without TiN template at oxygen pressures of 7×10^{-2} Pa and 13 Pa. The typical thicknesses of BST films were around 250 nm in this study. The detailed deposition procedures were described in Ref. 19.

To study TiN thickness dependence, the thickness of TiN template was controlled below 2 nm. The structural characterizations of the films were performed using X-ray diffraction (XRD) and reflection high-energy electron diffraction (RHEED). To investigate the dielectric properties, coplanar capacitors having a 12 μm gap between two Au/Cr square electrodes (750 μm × 750 μm) were fabricated. A precision LCR meter and a Joule–Thomson thermal stage were used for the dielectric measurements at various temperatures (100–320 K). The dielectric constant of BST films was estimated from the measured capacitance by using the model based on the conformal mapping technique developed by Vendik et al.[4]

3. Results and discussion

3.1 BST films directly deposited on *c*-Al₂O₃

Figure 2 shows the XRD θ–2θ patterns of BST films directly deposited on *c*-Al₂O₃ at different oxygen pressures. The BST film deposited at 13 Pa (that is in the typical pressure range for BST depositions[8),9),12)]) showed the polycrystalline nature. In addition, the film deposited at lower oxygen pressure of 7×10^{-2} Pa was also polycrystalline, although the orientation ratio was slightly different. The similar behavior was also observed for the films deposited on *r*-Al₂O₃. These results indicate that the oxygen pressure does not drastically influence the orientation of BST films and the epitaxial nucleation of BST does not easily take place on Al₂O₃, at least within the examined deposition conditions.

However, it is interesting to mention that the dielectric constant of polycrystalline films was higher when the oxygen pressure was lower. At room temperature, the dielectric constant of the film deposited at 7×10^{-2} Pa O₂ was estimated to be 480, while that of the film deposited at 13 Pa O₂ was 200. Although this difference can be due to several factors the main reason will be the difference in the porosity in the films as has been widely known that a higher deposition pressure more likely results in a porous structure.[20] Malic et al. reported the effect of the porosity on the dielectric constant of BST films fabricated by chemical solution deposition and showed that the porosity of the film drastically reduced the effective dielectric constant of the films.[5]

3.2 BST films deposited on *c*-Al₂O₃ with TiN sacrificial template

In order to grow BST films epitaxially on Al₂O₃, buffer layers (that match for both film and substrate) are often inserted.[21)–23)] Nevertheless, since the epitaxial growth of BST without any buffer layers has also been reported,[15),16)] the epitaxial growth on Al₂O₃ may be promoted only by the surface modification of Al₂O₃ instead of the insertion of additional thick buffer layers. Since the ABO₃-perovskite lattice consists of two types of cation-containing layers, i.e., AO and BO₂ along [100] direction, and AO₃ and B along [111] direction, the modification of Al₂O₃ surface by one of those cations with proper atomic configuration would work as the first atomic layer for the BST epitaxial growth. TiN is known to grow epitaxially on *c*-Al₂O₃ with (111) orientation at room temperature,[24] and the Ti configuration in BST (*hhh*) plane is a subset of that in TiN (*hhh*) plane. Therefore, even an ultra-thin TiN layer would be enough to promote the epitaxial growth of BST on *c*-Al₂O₃ with (111)-orientation.[19]

Figure 3 shows the RHEED images from *c*-Al₂O₃ surfaces covered with/without TiN layer. For 0.6 nm-TiN thickness (that is the value estimated from the average deposition rate of thick TiN films), the RHEED pattern was almost the same as that of the bare *c*-Al₂O₃ surface. Above this thickness, the streaks from epitaxial TiN surfaces were observed. **Figure 4** shows the XRD θ–2θ patterns of BST films deposited on *c*-Al₂O₃ with/without TiN layer. Although the film on *c*-Al₂O₃ without TiN layer was polycrystalline, the films on TiN layer-covered *c*-Al₂O₃ grew with (111)-orientation regardless of the inserted TiN thickness. The RHEED images shown in **Fig. 5** are of the films deposited on the thinnest (0.6 nm) and thickest (1.8 nm) TiN layer-covered *c*-Al₂O₃. As shown in the figures, BST epitaxially grew regardless of the inserted TiN thickness. The observed diffraction spots are corresponding to two kinds of epitaxial relationships of BST[2$\bar{1}\bar{1}$] ‖ Al₂O₃[11$\bar{2}$0] and BST[2$\bar{1}\bar{1}$] ‖ Al₂O₃[2$\bar{1}\bar{1}$0] [Fig. 5(c)]; namely, two (111) domains have 60° in-plane rotation angle each other. These relationships were also confirmed by XRD phi scans in our previous study.[19] The scanning electron microscope image of the epitaxial BST film (**Fig. 6**) showed the completely dense microstructure due to the epitaxial growth. In addition, the transmission electron microscopy analysis (not shown here) indicated that TiN template was absorbed by BST during the
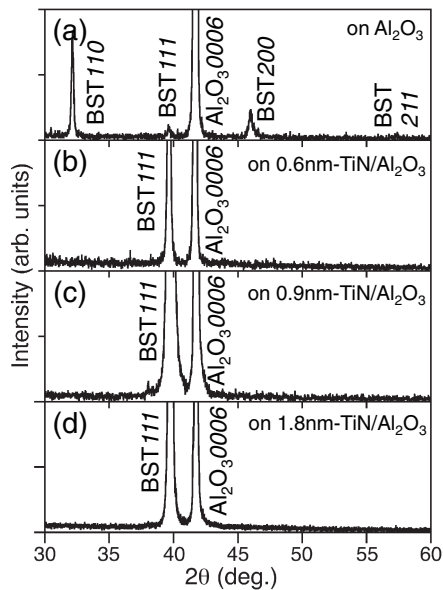
Fig. 4. XRD θ–2θ patterns of BST films on c-Al_2O_3 without TiN layer (deposited at 7×10^{-2} Pa) (a), on 0.6 nm-thick TiN-covered c-Al_2O_3 (b), on 0.9 nm-thick TiN-covered c-Al_2O_3 (c), and on 1.8 nm-thick TiN-covered c-Al_2O_3 (d).
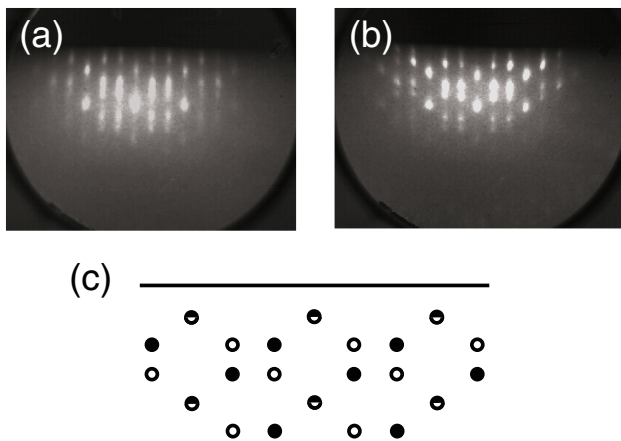

Fig. 5. RHEED images of BST films on 0.6 nm-thick TiN-covered c-Al_2O_3 (a) and on 1.8 nm-thick TiN-covered c-Al_2O_3 (b) in the c-$Al_2O_3[10\bar{1}0]$ azimuth. (c) shows the diffraction patterns in the same azimuth for two kinds of epitaxial relationships of BST$[2\bar{1}\bar{1}]$ || $Al_2O_3[11\bar{2}0]$ and BST$[2\bar{1}\bar{1}]$ || $Al_2O_3[2\bar{1}\bar{1}0]$ ($\bullet$, $\bigcirc$).

Fig. 6. Scanning electron microscope image of epitaxial BST film grown on 0.9 nm-thick TiN-covered c-Al_2O_3.

Fig. 7. Temperature dependence of in-plane dielectric constant of BST films measured at 1 MHz: Polycrystalline BST film on c-Al_2O_3 without TiN layer (deposited at 7×10^{-2} Pa) (a) and epitaxial BST films on 0.6 nm-thick TiN-covered c-Al_2O_3 (b) and on 0.9 nm-thick TiN-covered c-Al_2O_3 (c).

Fig. 8. Out-of-plane strain of epitaxial BST films on TiN-covered c-Al_2O_3 measured at room temperature.

deposition at high temperature in oxygen ambient; therefore, TiN template sacrificially worked as a first atomic layer for the (111)-epitaxial growth of BST on c-Al_2O_3.

Figure 7 shows the temperature dependence of dielectric constant of the films measured at 1 MHz. In this study, no significant frequency dispersion of the dielectric constant was observed in the frequency range of 10 kHz to 1 MHz. The dielectric constant of the epitaxial films was remarkably larger than that of the polycrystalline film without TiN template for all the temperature range, and the temperatures corresponding to the maximum dielectric constant of the epitaxial films were higher than that of the polycrystalline film and the Curie–Weiss temperature of BST ($x = 0.3$) (170 K). The former is basically attributed to the completely dense microstructure and the higher crystallinity of the epitaxial films. The latter, the shift of the
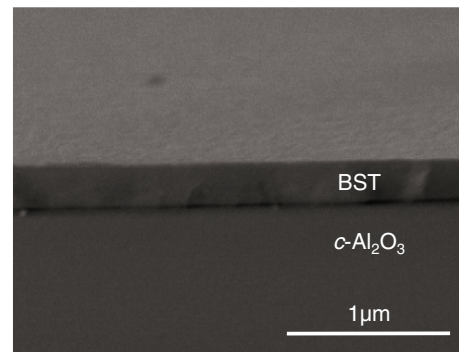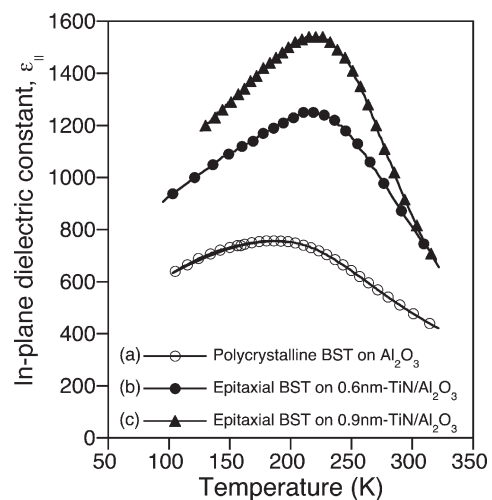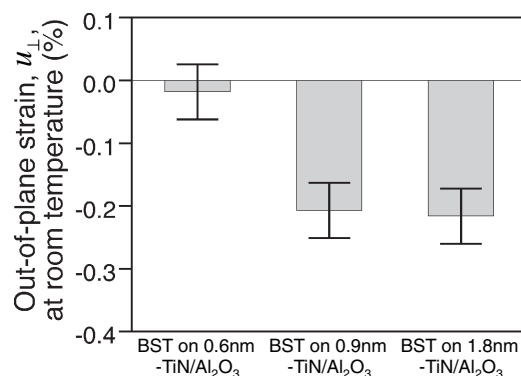
temperature corresponding to the maximum dielectric constant, represents the shift of the paraelectric to ferroelectric phase transition temperature by the strain induced in the films.[7),10),25)]

Figure 8 shows the measured out-of-plane strain $u_\perp$ of the films. It was found that the out-of-plane compressive strain was induced, and increased with increasing the TiN thickness. The strain in the epitaxial film is generally induced by the biaxial

stress owing to the mismatch of the lattice constant and/or the thermal expansion coefficient between the film and the substrate. In the case of the (111)-epitaxial growth of BST, we found in our previous study[26),27)] that the lattice mismatch is efficiently released during the growth due to the island nuclei on the growing surface; therefore, the strain in the present films having the total thickness of 250 nm is not able to be explained by the lattice mismatch as a major reason. On the other hand, the mismatch of the thermal expansion coefficients between BST and c-Al₂O₃ will induce the strain in the film during cooling down from the deposition temperature, which is valid for a wide range of film thickness unless the thickness of the film is comparable to that of the substrate.[28),29)] Assuming that the film is fully relaxed from the lattice mismatch at the deposition temperature, the in-plane strain at certain temperature $u_\parallel(T)$ is expressed by:

$$u_\parallel(T) = (T - T_{DT})(\alpha_{c\text{-Al}_2\text{O}_3} - \alpha_{BST}), \quad (1)$$

where T_{DT} is the deposition temperature, $\alpha_{c\text{-Al}_2\text{O}_3}$ and α_{BST} are the thermal expansion coefficients of c-Al₂O₃ ($\approx 7 \times 10^{-6}$/K along the a-axis) and BST ($\approx 10 \times 10^{-6}$/K). Based on the Poisson effect, the out-of-plane strain at certain temperature $u_\perp(T)$ is described as follows:

$$
\begin{aligned}
u_\perp(T) &= \frac{-2\nu_{111}}{1 - \nu_{111}} u_\parallel(T) \\
&= \frac{4s_{11} + 8s_{12} - 2s_{44}}{4s_{11} + 8s_{12} + s_{44}}(T - T_{DT})(\alpha_{c\text{-Al}_2\text{O}_3} - \alpha_{BST}), \quad (2)
\end{aligned}
$$

where ν_{111} is the Poisson ratio for (111)-oriented BST films and s_{ij} are the elastic compliance coefficients.[30)] With the coefficients given for BST,[10),31),32)] the Poisson effect results in the opposite sign of strain for in-plane and out-of-plane directions. For the case of BST films on c-Al₂O₃, the tensile strain will be induced in the in-plane below the deposition temperature due to the mismatch of the thermal expansion coefficients; therefore, the out-of-plane strain becomes compressive. At room temperature, the out-of-plane compressive strain of around 0.1% is expected when there is no strain owing to the lattice mismatch. As compared with the prediction, the size of the compressive strain of the BST films observed at room temperature was somewhat smaller and lager for the films on 0.6 nm and >0.6 nm-thick TiN templates, respectively. At this time, the exact reason of such thickness dependence is not clear. It might be due to the additional minor impact of the lattice mismatches between BST and TiN and between TiN and c-Al₂O₃ if the layers were not completely relaxed during the growth. Further investigations are needed in the future.

The dielectric constant of the strained (111)-epitaxial BST films in the paraelectric phase can be predicted from the Landau expansion of the free energy as,

$$
\begin{aligned}
\frac{1}{\varepsilon_\parallel} &= \frac{T - T_0}{C} - 2\varepsilon_0 \frac{4Q_{11} + 8Q_{12} + Q_{44}}{4S_{11} + 8S_{12} + S_{44}} u_\parallel(T) \\
\frac{1}{\varepsilon_\perp} &= \frac{T - T_0}{C} - 2\varepsilon_0 \frac{4Q_{11} + 8Q_{12} - 2Q_{44}}{4S_{11} + 8S_{12} + S_{44}} u_\parallel(T), \quad (3)
\end{aligned}
$$

where $\varepsilon_\parallel$ and $\varepsilon_\perp$ are the in-plane and out-of-plane dielectric constant, ε_0 is the permittivity of vacuum, T_0 is the Curie–Weiss temperature, C is the Curie–Weiss constant, and Q_{ij} are the electrostrictive constants.[33)] When the in-plane strain is tensile (thus, the out-of-plane strain is compressive) as in the present study, the in-plane dielectric constant, i.e., the measured component, becomes larger from Eq. (3). In addition, the temperature corresponding to the maximum in-plane dielectric constant will be also increased by around 55 K from the Curie–

Weiss temperature of BST ($x = 0.3$) ($T_0 = 170$ K). The observed increases were around 50 K, whish reasonably agreed with the prediction with the consideration of the variation of the reported values for the coefficients.[10),31),32)]

4. Conclusions

In this paper, the comprehensive study of the BST films epitaxially grown on c-Al₂O₃ using TiN templates was reported. An ultra-thin TiN template sacrificially acted as a first atomic layer for the (111)-epitaxial growth of BST on c-Al₂O₃. The epitaxial films showed the significantly larger dielectric constant than the polycrystalline films, and the temperature corresponding to the maximum dielectric constant was higher than the unstrained bulk BST. The former is due to the dense microstructure and higher crystallinity of the epitaxial films, and the latter is basically due to the in-plane tensile strain induced by the mismatch of the thermal expansion coefficients between the BST film and the c-Al₂O₃ substrate.

References

1) O. G. Vendik, E. K. Hollman, A. B. Kozyrev and A. M. Prudan, *J. Supercond.*, 12, 325–338 (1999).
2) A. K. Tagantsev, V. O. Sherman, K. F. Astafiev, J. Venkatesh and N. Setter, *J. Electroceram.*, 11, 5–66 (2003).
3) A. Vorobiev, P. Rundqvist, K. Khamchane and S. Gevorgian, *Appl. Phys. Lett.*, 83, 3144–3146 (2003).
4) O. G. Vendik, S. P. Zubko and M. A. Nikolski, *Tech. Phys.*, 44, 349–355 (1999).
5) B. Malic, M. Vukadinovic, I. Boerasu, M. Mandeljc, E. Ion, M. Kosec, V. O. Sherman, T. Yamada and N. Setter, *Integr. Ferroelectr.*, 93, 119–125 (2007).
6) T. Satoh, M. Ogawa and M. Konno, *J. Ceram. Soc. Japan*, 106, 1151–1154 (1998).
7) N. A. Pertsev, A. K. Tagantsev and N. Setter, *Phys. Rev. B*, 61, R825–R829 (2000).
8) C. L. Canedy, H. Li, S. P. Alpay, L. Salamanca-Riba, A. L. Roytburd and R. Ramesh, *Appl. Phys. Lett.*, 77, 1695–1697 (2000).
9) H. Li, A. L. Roytburd, S. P. Alpay, T. D. Tran, L. Salamanca-Riba and R. Ramesh, *Appl. Phys. Lett.*, 78, 2354–2356 (2001).
10) Z. G. Ban and S. P. Alpay, *J. Appl. Phys.*, 91, 9288–9296 (2002).
11) J. H. Haeni, P. Irvin, W. Chang, R. Uecker, P. Reiche, Y. L. Li, S. Choudhury, W. Tian, M. E. Hawley, B. Craigo, A. K. Tagantsev, X. Q. Pan, S. K. Streiffer, L. Q. Chen, S. W. Kirchoefer, J. Levy and D. G. Schlom, *Nature*, 430, 758–761 (2004).
12) T. Yamada, K. F. Astafiev, V. O. Sherman, A. K. Tagantsev, P. Muralt and N. Setter, *Appl. Phys. Lett.*, 86, 142904 (2005).
13) J. Schubert, O. Trithaveesak, A. Petraru, C. L. Jia, R. Uecker, P. Reiche and D. G. Schlom, *Appl. Phys. Lett.*, 82, 3460–3462 (2003).
14) K. Yazawa, S. Yasui, H. Morioka, T. Yamada, H. Uchida, A. Gruverman and H. Funakubo, *J. Ceram. Soc. Japan*, 118, 659–663 (2010).
15) D. Rafaja, J. Kub, D. Šimek, J. Lindner and J. Petzelt, *Thin Solid Films*, 422, 8–13 (2002).
16) E. A. Fardin, S. Holland, K. Ghorbani and P. Reichart, *Appl. Phys. Lett.*, 89, 022901 (2006).
17) T. Ostapchuk, J. Petzelt, V. Železný, A. Pashkin, J. Pokorný,

I. Drbohlav, R. Kužel, D. Rafaja, B. P. Gorshunov, M. Dressel, Ch. Ohly, S. Hoffmann-Eifert and R. Waser, *Phys. Rev. B*, 66, 235406 (2002), and references therein.

18) I. Boerasu, B. Malic, M. Mandeljc, M. Kosec, V. Bobnar, V. Sherman, T. Yamada and N. Setter, Proc. 41st International Conference on Microelectronics, Devices and Materials, Bled, Slovenia, September (2005), pp. 107–112.

19) T. Yamada, P. Muralt, V. O. Sherman, C. Sandu and N. Setter, *Appl. Phys. Lett.*, 90, 142911 (2007).

20) A. Infortuna, A. S. Harvey and L. J. Gauckler, *Adv. Funct. Mater.*, 18, 127–135 (2008).

21) H. Li, J. Finder, Y. Liang, R. Gregory and W. Qin, *Appl. Phys. Lett.*, 87, 072905 (2005).

22) C. H. Lei and G. Van Tendeoo, *Philos. Mag. Lett.*, 82, 433–442 (2002).

23) R. Ott and R. Wördenweber, *Physica C*, 372, 540–542 (2002).

24) A. Sasaki, W. Hara, A. Matsuda, S. Akiba, N. Tateda and M. Yoshimoto, *Nucl. Instrum. Methods Phys. Res. B*, 232, 305–311 (2005).

25) K. Abe, *J. Ceram. Soc. Japan*, 109, S58–S64 (2001).

26) T. Yamada, T. Kamo, D. Su, T. Iijima and H. Funakubo, *Ferroelectrics*, 405, 262–267 (2010).

27) T. Yamada, T. Kamo, H. Funakubo, D. Su and T. Iijima, *J. Appl. Phys.*, in press (2011).

28) T. Fujisawa, H. Nakaki, R. Ikariyama, H. Morioka, T. Yamada, K. Saito and H. Funakubo, *Appl. Phys. Express*, 1, 085001 (2008).

29) S. Utsugi, T. Fujisawa, Y. Ehara, T. Yamada, S. Yasui, M.-T. Chentir, H. Morioka, T. Iijima and H. Funakubo, *J. Ceram. Soc. Japan*, 118, 627–630 (2010).

30) W. A. Brantley, *J. Appl. Phys.*, 44, 534–535 (1973).

31) E. Poindexter and A. A. Giardini, *Phys. Rev.*, 110, 1069 (1958).

32) N. A. Pertsev, A. G. Zembilgotov, S. Hoffmann, R. Waser and A. K. Tagantsev, *J. Appl. Phys.*, 85, 1689–1701 (1999).

33) A. K. Tagantsev, N. A. Pertsev, P. Muralt and N. Setter, *Phys. Rev. B*, 65, 012104 (2001).

Tomoaki Yamada received his M.S. and Ph.D. degrees in material science and engineering from Tokyo Institute of Technology, Japan, in 2001 and 2003, respectively. In 2004, he joined the ceramics laboratory of Swiss Federal Institute of Technology at Lausanne (EPFL), Switzerland. In 2008, he became an assistant professor under the global COE program in Tokyo Institute of Technology, Japan. Since 2010 he is an associate professor in Nagoya University, Japan. His domains of experience and expertise are metal oxide thin films and devices, especially with focus on the manipulation of epitaxial growth, nano-structured interfaces, and characterizations and applications of these hetero-structures.